# AFCI Quarterly Input – UNLV
# April through June, 2004

## 1.0 University of Nevada, Las Vegas (UNLV)

**UNLV Transmutation Research Program**. The University of Nevada, Las Vegas supports the AFCI through research and development of technologies for economic and environmentally sound refinement of spent nuclear fuel. The UNLV program has four components: infrastructure, international collaboration, student-based research, and management and program support.

- The following 13 papers were presented at the American Nuclear Society Student Conference in Madison, WI, April 1-3, by UNLV students:
  - Tan, T., Clarksean, R., Chen, Y., and Hsieh, H.-T., *Design and Numerical Simulation of an Induction Skull Melting Process*, Department of Mechanical Engineering (Task 1)
  - George, A. and Schill, R.A., *Preparation Studies for Secondary Electron Emission Experiments on Superconducting Niobium*, Department of Electrical and Computer Engineering (Task 2)
  - Sama, S. *Stress Corrosion Cracking and Localized corrosion in Alloy HT-9*, Department of Mechanical Engineering (Task 4)
  - Prabhakaran, R., *Environmental Effects on a Candidate Structural Material for Transmutation Application*, Department of Mechanical Engineering (Task 4)
  - Hossain, M., *Stress Corrosion Cracking of Structural Target Material Alloy EP- 823*, Department of Mechanical Engineering (Task 4)
  - Selvaraj, V. and Gudipati, P.P.K., *Cracking of Target Structural Materials in Different Environments*, Department of Mechanical Engineering (Task 4)
  - Li, G., *3-D Thermal hydraulic and Chemical Kinetics in LBE Loop Fittings*, Department of Mechanical Engineering (Task 5)
  - Renno, J.M. and Mauer, G.F., *Remote Transmuter Fuel Fabrication*, Department of Mechanical Engineering (Task 9)
  - Kujatla, S.R., Potluri, V.N. and Yarlagadda, B., *Temperature Effect on Mechanical Properties of Target Structural Materials*, Department of Mechanical Engineering (Task 10)
  - O' Brien, R. and Culbreth, W., *Critically and Heat Transfer Analysis of a Np/Pu Mixture*, Department of Mechanical Engineering (Task 11)
  - Bakker, E. and Culbreth, W., *Criticality and Thermal Analysis of Separated Actinides in Transmutation*, Department of Mechanical Engineering (Task 11)
  - Sadineni, S.B., *Benchmarking Photo-Neutron Predictions from MCNPX*, Department of Mechanical Engineering (Task 12)
  - Lowe, D., Culbreth, W., and Wilcox, T., *MCNPX on Heterogeneous Clusters Using PVM and MPI*, Department of Mechanical Engineering (Task 12)
  - Ma, J., Guo, P., Rahman, S., Zhang, J., Li, N. and Fu, B., *Enhancement of Oxygen Transfer in Liquid Lead-Bismuth Eutectic by Natural Convection*, Department of Mechanical Engineering (Task 13)
  - Marthandam, V., *Residual Stress Measurments and Metallurgical Characterization of*

*Target Structural Materials*, Department of Mechanical Engineering (Task 14)

Dronavalli, S.B., *Comparative Analyses of Residual Stresses in Target Structural Materials*, Department of Mechanical Engineering (Task 14)

Rodrigo, C.P., Silva, C., Johnson, A.L., Hemmers, O., Perry, D., and Lindle, D.W., *Evaluation of Fluorapatite as a Waste Form*, Department of Chemistry (Task 16)

- Fourteen proposals for graduate student research starting Fall term 2004 were submitted to the DOE Program Advisory Committee. The top seven ranked new proposals and two proposals on continuing projects were approved by the UNLV Finance Committee.

## 1.1 Infrastructure Augmentation

### *1.1.1 Infrastructure Augmentation Scope*

The infrastructure augmentation component of the UNLV Transmutation Research Program enhances UNLV's research staff, facilities, and academic programs to increase the ability of the university to perform AFCI research.

### *1.1.2 Infrastructure Augmentation Highlights*

- **Academic Programs**. Prof. Ken Czerwinski was appointed the director of the new Ph.D. program in Radiochemistry. The program will be offered Fall term 2004. The University and Community College System of Nevada Board of Regents approved the Materials and Nuclear Engineering M.S. Degree Program proposal on June 4, 2004. The new degree program in the Mechanical Engineering Department will be offered Fall term 2004.
- **Facilities Progress Update**. Remodeling of MSM 173 for the actinide chemistry laboratory continued on schedule. Target completion date is end of July. An Ion Mill system was installed in the Electron Microscopy Sample Preparation laboratory. The laboratory is now equipped to allow on-site preparation of almost any sample to be encountered in the TRP research efforts.

## 1.2 International Collaboration

### *1.2.1 International Collaboration Scope*

The international collaboration component of the UNLV Transmutation Research Program enhances UNLV's breadth of scientific and scholastic experience. University collaboration is also an efficient conduit for international collaboration that benefits the national AFCI program. UNLV has ongoing relationships with the Khlopin Radium Institute (KRI) in St. Petersburg, Russia; the Institute for Physics and Power Engineering (IPPE) in Obninsk, Russia; and members of the International Molten Metal Advisory Committee (from Sweden, Germany, Belgium, and Italy).

## 1.3 Student Research

### *1.3.1 Student Research Scope*

The Student Research component is the core of the UNLV Transmutation Research Program with steadily increasing funds as the program evolves and capability expands. The milestones, schedules, and deliverables of the student research projects are detailed in the individual research proposals. UNLV currently has 19 student research tasks that include 36 graduate students and involve 26 faculty members. The tasks are divided below in terms of their research area: fuels, separations, and transmutation sciences.

### *1.3.2 Student Research Highlights*

**FUELS TECHNOLOGY**

**Metallic Fuel Pins (Task 1) Highlights.**

- Researchers attended the ICONE12 Conference in Crystal City, Arlington, Virginia (Washington, D. C.) from April 25 to 29 and presented two papers: "Numerical Simulation of the Casting Process of a Mold for Casting a Metallic Fuel Pin Using FIDAP" and "Design and Numerical Simulation of an Induction Skull Melting Process."
- Work concluded on a transient model for variable (linear increasing) power input for the ANL-W induction skull melting furnace.
- The final report was submitted.
- Task completed.

**Remote Fuel Fabrication (Task 9) Highlights.**

- Further refinements on Concepts and Methods for Vision-Based Hot Cell Supervision and control, focusing on rule-based object recognition (Ph.D. Graduate Jae-Kyu Lee). Ms. Caroline Wiejak, an exchange student from the ESIEE in Marne-la-Vallee, France is continuing with the image analysis effort. To date, she has transferred Lee's code to Matlab, and is presently expanding its application to more complex 3D shapes.
- Graduate student Jamil Renno refined and detailed his simulations of more complex fuel manufacturing and fuel pin assembly scenarios using hot cell robots. He also begun working on the manufacturing modeling of metal fuels.

**Interaction between Metal Fission Products and TRISO Coating Materials (Task17) Highlights.**

- Principal Investigator and graduate student traveled to Würzburg, Germany to perform research at the University of Würzburg during the summer while laboratory is being renovated at UNLV.
- Student training continued, including working with the ultra-high vacuum apparatus and advanced principles of photoelectron spectroscopy, literature search, and Pd/SiC and Ag/SiC interfaces.
- Optimized experimental setup (software, sample heating stage, X-ray source water cooling, electrical grounding, Pd evaporator, UV lamp operation).
- Performed test and calibration experiments (XPS and UPS) on a Au foil reference.
- Performed first XPS experiments on a commercial SiC-6H(0001) single crystal surface. Surface shows strong Si, C, and O signals, as well as Cr, F, and Ca contaminants from the polishing process. Sample annealing up to 780 C reduces the O, Ca, and F surface contamination.
- Due to technical aspects with the metal evaporator geometry, it was decided to begin with Pd/SiC interface studies (as opposed to Ag/SiC). The metal needs to be evaporated from an electron-beam evaporator in an "overhead geometry", which is easier with Pd than with Ag. The experience gained with Pd evaporation will thus be very helpful for a successful Ag evaporation.

**Dissolution, Reactor, and Environmental Behavior of $ZrO_2$-MgO Inert Fuel Matrix (Task19) Highlights.**

- Contract in the process of being finalized with collaborators at Ben-Gurion University.
- Principal Investigator met with collaborators at ANL-West and BNL to discuss inert matrix fuels.
- PI participated in the IAEA project on Inert Matrix Fuels in Vienna, Austria.

## SEPARATIONS TECHNOLOGY

**Systems Engineering Model (Task 8) Highlights.**

- The TRPSEMPro was tested on some known case studies. Additional programming bugs have been identified by the collaborators at ANL. Additional students have been added to the task for the summer to assist in the programming effort to resolve these bugs.
- Work continues on resolving implementation issues.
    - The system model is being revised to allow optimization and analysis of smaller test scenarios to allow analysis of systems where some model components are still in development.
    - The connection between parameter ranges and DOE is not physically linked. Therefore the definition from the "Parameter" field is not passing the values into the DOE process for multiple-run scenarios.
- The systems engineering interface is being modified to allow multiple runs by inputting the design matrix directly.
- Work continued on the integration of the multiple-run module. Current system can be used to setup the optimization processing for benchmark problems. The implementation of the multiple-run modules is still under development.

**Criticality and Heat Transfer Analyses of Separations Processes (Task 11) Highlights.**

- Determination of maximum allowable container size and mass for a mixture of minor actinides without curium in oxide form was completed.

**Immobilization of Fission Iodine (Task 15) Highlights.**

- Reassembly of the fuel rod dissolution simulator was completed. High recovery of iodine from this system was demonstrated. The effect of $NO_x$ is being reexamined.
- Using the grease-free system, fuel rod dissolution experiments were repeated with peat/$Ca(OH)_2$.
- Additional experiments were done with the iodine generator and breakthrough curves were measured for different ratios of peat to $Ca(OH)_2$.
- Additional data on the reaction of peat with iodine was obtained. Time series experiments were completed that indicate a pseudo first order reaction of iodine with peat.
- Several experiments with peat and iodate were conducted. It was demonstrated that iodate is reduced to iodide by the peat at high pH. Experiments at pH of 2-9 demonstrated that 5-30% of the iodine (from the iodate ) is incorporated into the peat has

been conducted. The incorporation of iodine from iodate has been quantified by pyrolysis GC/MS.
- Different ways to present and analyze breakthrough curves for iodine on FCC and Peat are being examined.

**Fluorapatite Waste Forms (Task 16) Highlights.**

- Synthesized Fluorapatite powder and measured an IR spectrum of a sample.
- Prepared two more H-apatitie samples using refluxing method to check the thermodynamic effects on the crystalline character/shape of the samples. Obtained XPS, FTIR and SEM/EDS data of these samples.
- Synthetic Fluorapatite samples prepared using dissolved hydroxyapatite and ZnCl2 solution. Obtained IR data (using IR image) for four samples. Analyzed the data that was obtained to determine the optimum fabrication parameters for systems examined.
- Three samples prepared of hydroxyapatite containing fluorine (using refluxing, without refluxing and using precipitation process). SEM, IR and XPS data obtained of those samples.
- Fluorapatite and strontium containing Fluorapatite synthesized and annealed at 1200 C.

**TRANSMUTATION SCIENCES**

**Niobium Cavity Fabrication Optimization (Task 2) Highlights.**

- Position detector card and software has been loaded in the computer.
- Detector, electron gun, cryostat, and manipulator arm installed in UHV vacuum chamber
- With cryostat on, $5x10^{-9}$ Torr was achieved.
- Secondary electron emission Monte Carlo code has been rewritten and placed on a more user friendly source platform for future modifications relevant to the experiment to be conducted.
- LANL cleaned niobium samples received from LANL. Cornell cleaned niobium samples have been mailed.
- Small pinhole has been identified in the adjustable bellows. Special vacuum glue has been acquired and applied temporarily fixing the leak.
- InGa is not acting as a good thermal conductor and needs to be replaced with a different product so that the piece under testing will reach superconducting temperatures.
- Temperature diode on cryostat is being calibrated.

**LBE Corrosion of Steel (Task 3) Highlights.**

- Design work on the molten metal small experiments facility (in room CHE 112) continued.
- Raman spectroscopy of corroded steel samples continued.
- Project students were trained on Xray Photoelectron Spectroscopy to assist with surface chemistry analysis.
- Final technical report being prepared for submittal.
- Task completed. Follow-on research funded under Task 18 (see below).

**Environment-induced Degradation of Materials (Task 4) Highlights.**

- Stress corrosion cracking (SCC) tests under controlled electrochemical potential ($E_{cont}$) were ongoing using the slow-strain-rate testing technique. SCC tests were also in progress without $E_{cont}$.
- SCC testing using self-loaded (C-ring and U-bend) specimens was in progress in high-temperature aqueous solutions for different exposure periods.
- Fractographic evaluations by scanning electron microscopy were continued. Microstructural analyses by optical microscopy were also continued.

**Neutron Multiplicity Measurements of AAA Target/Blanket Materials (Task 6) Highlights.**

- MCNPX models of the Neutron Multiplicity Detector System (NMDS) have been completed for 3 configurations for upcoming experiments at the Idaho Accelerator Center.
- A set of experiments was conducted using 1 to 6 layers of lead in the NMDS.
- Work continued with the Khlopin Radium Institute to determine the cause of computer lock-ups with our data acquisition program.

**Dose Conversion Coefficients (Task 7) Highlights.**

- Completed all radionuclides that had complete data files.
- Completed the organization of the radionuclides that are missing data.
- Began looking at producing these nuclides at Idaho State University.

**Properties of Alloy EP-823 (Task 10) Highlights.**

- Mechanical testing involving Alloys EP-823, HT-9 and 422 was completed at ambient and elevated temperatures in the presence of nitrogen using the MTS unit.
- Metallography and fractography are in progress involving all tested tensile specimens using optical microscopy and scanning electron microscopy (SEM), respectively.
- Tensile specimens tested at ambient and elevated temperatures are currently being analyzed for metallographic and fractographic evaluations. Analyses of tensile data have been completed.
- A batch of sectioned tensile specimens (Type 422 SS) was sent to FEI Corporation for electropolishing and subsequent evaluation of defects by TEM.

**Oxygen Sensing in LBE (Task 13) Highlights.**

- 380 hour corrosion testing on three metal samples, Tungsten, Niobium and Molybdenum, was completed. No corrosion was observed under the implemented oxygen control methods.
- Sensor sensitivity under different gas input processes was examined.
- Sensor lifetime at 600$^{o}$C was examined. The three sensor systems survived for ~300 hours.
- 3-D simulation of the Oxygen Sensor Test Bed system using FLUENT is almost finished.
- Oxygen sensor response to addition of $O_2$ and addition of $H_2$ was tested.
- The Oxygen Control System (from KALLA, FZK) was installed. Training on the system was completed.

**Positron Annihilation Spectroscopy (Task 14) Highlights.**

- A second set of residual stress measurements was completed at the Atomic Energy of Canada Limited (AECL) using the neutron diffraction technique. Data analyses are in progress.
- Residual stress measurements on cold-worked and welded specimens by ring-core method have been completed. at the Lambda Research Laboratory. Data analyses are ongoing.
- TEM sample preparations are in progress to characterize imperfections/dislocations due to plastic deformation and welding.
- Residual stress measurements on tensile specimens of Type 304L stainless by the positron annihilation spectroscopic (PAS) technique were in progress at ISU for developing calibration curves. PAS tests using welded specimens of Alloy HT-9 were also ongoing at ISU.

**Corrosion Mechanisms and Kinetics of Steels in Lead-Bismuth Eutectic (Task 18) Highlights.**

- Design of the Small Experiments Facility has been initiated. Room CHE 112C will be renovated to allow work with molten lead and lead-bismuth.
- Upgrades of the XPS system completed.

### 1.3.3 Student Research Technical Summary

**FUELS TECHNOLOGY**

**Metallic Fuel Pins (Task 1).**

Incorporating volatile actinides, mainly americium into a metallic fuel pin (MFP) has been a serious problem due to americium's high vapor pressure. An Induction Skull Melting (ISM) system was identified by Argonne National Laboratory (ANL) as a potential furnace design to cast MFPs. The main phenomena in this system include: induction melting process, casting process and mass transfer process of americium.

The induction melting and casting problems were analyzed numerically through coupling the commercial finite element CFD package FIDAP (Fluent, Inc.) with FORTRAN and Perl subroutines. Various values of the material properties and input parameters were employed in the simulations and the results are compared in order to provide a better parameter estimation for the system design and real operation.

The model has shown the ability to calculate the induction-heating field for typical geometries (coil, crucible, melt). Rapid heating is typically experienced in the region indicated by the high fluxes, resulting in the melting of the material within the ISM. And the "skin effect" was observed and finally a "skull" was formed due to the presence of the cooling system. These conclusions coincide with the theoretical analysis and the numerical and experimental results.

The maximum value of the induction heating power deposition keeps increasing with the current value or current density and the current frequency. Hence, one can draw a conclusion that the current value and the current frequency have a relatively larger impact on the induction heating process.

*Energy Storage Ability of the Mold*

When the melt flows into the mold there two issues to consider: the flow and initial solidification of the melt during the initial rapid transient and the final cooling and solidification of the melt once the flow stops. If the mold has adequate thermal mass, this implies the melt within the mold will be completely solidified and no additional cooling will be needed. If there were no adequate thermal mass, then active or passive cooling would be necessary to cool and solidify the melt within the mold.

The bigger the mold outer radius is, the more energy can be stored in the mold. The stainless steel mold has the greatest storing ability whereas the quartz glass mold has the smallest one. On the other hand, for a bigger mold the solidification progress will take a longer time. This will lead to a low efficiency and is not anticipated in production. Finally an outer radius of 0.008 m is selected for the mold by ANL. This value ensures that the energy stored by the mold is larger than the minimum heat needs to be absorbed from the melt and a fast solidification for all the three kind of mold materials.

*Simple Solidification Process*

The analysis of "simple" or "pure" solidification considers the mold to be filled with molten material before the solidification begins. The inlet boundary condition can be either constant velocity (simplified injection), or a constant pressure condition (realistic boundary condition for injection casting). This type of analysis gives insight into the time scales one must consider for the solidification of the melt once it is in the mold. In the "simple" solidification is a solidification process in which the interface of the melt and the solidified melt moves in a radial direction. Note that the inlet temperature of the melt is set to a constant temperature representative of the superheat of the melt.

Figure 3.1 shows how the flow increases in velocity and then starts to decrease in velocity as the melt starts to solidify. A constant pressure boundary condition is representative of the injection casting process where pressure is suddenly ramped up, forcing the molten material into a mold. The flow starts of nearly in a plug flow shape, slowly moves to more of a parabolic shape, and the remains nearly parabolic as the total flow decreases as the melt solidifies towards the center of the geometry.

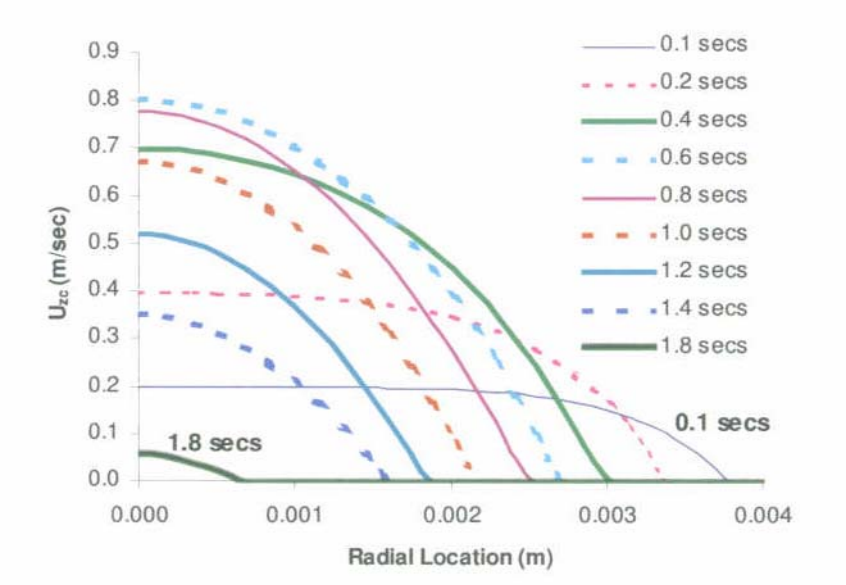


Figure 3.1. Axial velocity profile for constant inlet pressure of 20 kPa (Mold temperature = 400 $^{o}$C, initial melt temperature = 1500 $^{o}$C, interfacial heat transfer coefficient = 2,000 W/m2-K)

*Casting Process*

The single-fluid Volume of Fluid (VOF) technique was used in the casting process and phase change was considered at the same time. Results coincide with theoretical analysis. From the calculations, it was found that a larger value of the convection heat transfer coefficient will lead to a steeper slope. If the h value is too small, the solidification will not take place at the head of the molten, which means the slope is behind the filling head and it will take a longer time for all the molten metal in the mold to solidify.

The main difference between the VOF-solidification process and the "pure" solidification is the slopes. The flat interface of the "pure" solidification is because it was assumed the molten metal has filled the whole mold before the solidification took place, so there is almost no temperature difference in the wall of the mold. Moreover, there is no filling "head" and in turns there is no time difference for solidifying along the mold. From the results, one can draw a conclusion that the casting process can be analyzed by studying the "pure filling" and "pure solidification" process separately.

*Conclusions and Recommendations*

After considering the heating mechanisms, casting issues, crucible design and issues related to the mass transport of americium, an ISM system was selected for melting the feedstock and casting fuel pins containing high vapor pressure actinides (americium). The finite element commercial software (FIDAP) was used to simulate the induction melting process and the casting process. Phase change is considered both in the heating and in the solidification process. Various factors and properties are studied, such as boundary conditions and initial conditions, output current, frequency of the current, main dimensions of the system, mold preheating

temperature, heat transfer coefficient and mold material. As shown in simulated results, several conclusions can be drawn:

- The design of the system has great impact on the induction melting process. In order to obtain high heat efficiency, the coils group number can be designed as many as possible and the coils are located as near to the crucible as possible.
- The induction melting process is sensitive to the electrical factors and properties (Current density; frequency and output power). Through the control of these values one can control the melting process. The thermal properties of the feedstock and the crucible material are also important in the heating process.
- A direct Inductive Heating (IH) has a much higher efficiency than an indirect IH. In order to form the "skull", a low temperature and good thermal conductivity of the coolant is necessary.
- A Volume of Fluid (VOF)-Solidification process can be "divided" to a filling process and a solidification process and be studied respectively, especially for a case of low convective heat transfer coefficient value.
- A constant filling pressure is expected rather than a constant velocity in the casting process.
- Mold material, mold preheated temperature, inlet pressure, and heat transfer coefficient have relative large effects to the casting process. The following recommendations are made for future work:
    - Employ turbulent model for the inductive self-stirring effect in the induction melting process.
    - Study on the mass transfer process of americium and analyze the control methods for decreasing the transfer efficient.

**Remote Fuel Fabrication (Task 9).**

*Hot Cell Robot Dynamics Analysis*

*Robot Control and Kinematics*

The robot controller is implemented using MATLAB Simulink (see Fig 3.2). The block labeled ("Waellischmiller") connects the MATLAB© environment with the MSC.visualNastran© environment. The dynamic environments of MSC.visualNastran© feeds back the joint angles and joint angular velocities to Simulink, where the control agorithm is implemented. The simulation provides realistic dynamics modeling of all moving parts and the robots.

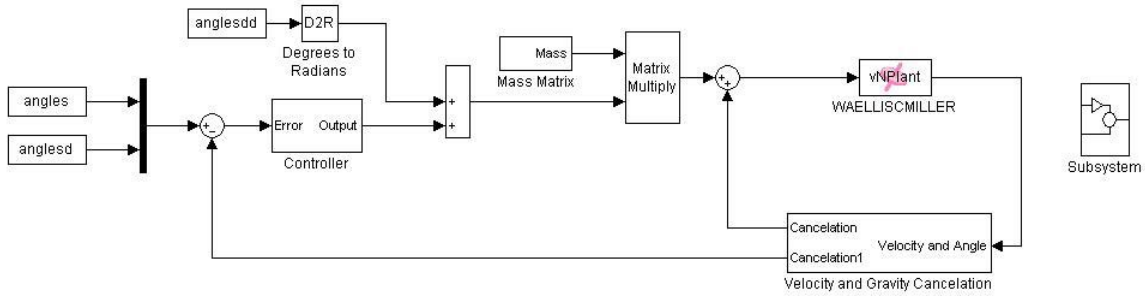


Figure 3.2. Computed Torque method implemented in MATLAB

*Case Study of Hot Cell Throughput*

The throughput of the powder process hot cell designed and described in earlier reports was studied. The powder process cell contains the following equipment:

1. Powder Pellet Press
2. Sintering Oven with Conveyor Belt
3. Grinder
4. V-Tray and Cladding Tube

The pellets are moved within the hot cell using two manipulators. Each manipulator has 6 joints, which allows it to reach any arbitrary point within its workspace with any orientation. Fig. 3.3 shows the material flow in the hot cell:

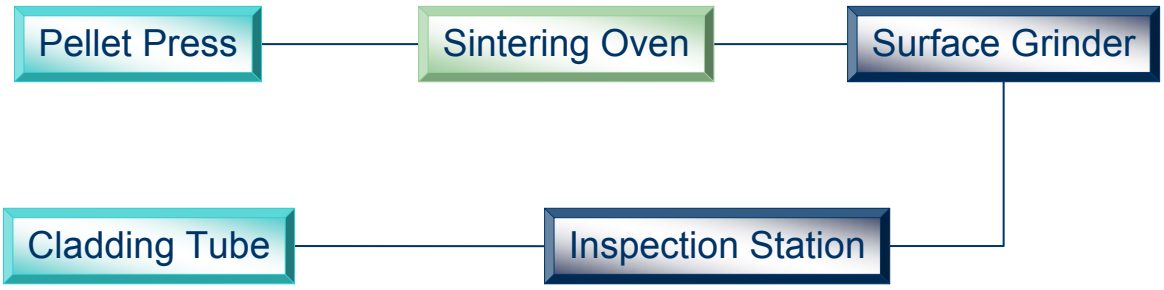


Figure 3.3. Material Flow in Hot Cell.

*Throughput Study*

In consideration of criticality concerns, no more than 30 pellets are assumed present in the hot cell at close proximity at the same time. The maximum permissible acceleration of a pellet is assumed to be 20 $m/s^2$ (Approx. twice earth gravity). If the trajectory of a pellet is planned so that its acceleration doesn't exceed 20 $m/s^2$, then the robot dynamics equations can be solved, and the controller can be programmed to keep the manipulator accelerations within the specified bounds.

Applying the above constraint on pellet motion, it will take 6 seconds to move a single pellet from the pellet press to the boat (placed on a conveyor belt for sintering). Another 4 seconds are

needed to travel back to get another pellet. Loading all 30 pellets will thus take 296 seconds. Our hot cell simulation was performed with 5 pellets, which theoretically need 50 seconds to be moved according to the schedule developed above. The simulation showed a total duration of 52 seconds, with the additional time due to controller delay. Fig. 3.4 shows the manipulator placing a pellet in the boat before sintering. The pellet acceleration was monitored and never exceeded 20 m/s$^2$ as designed.

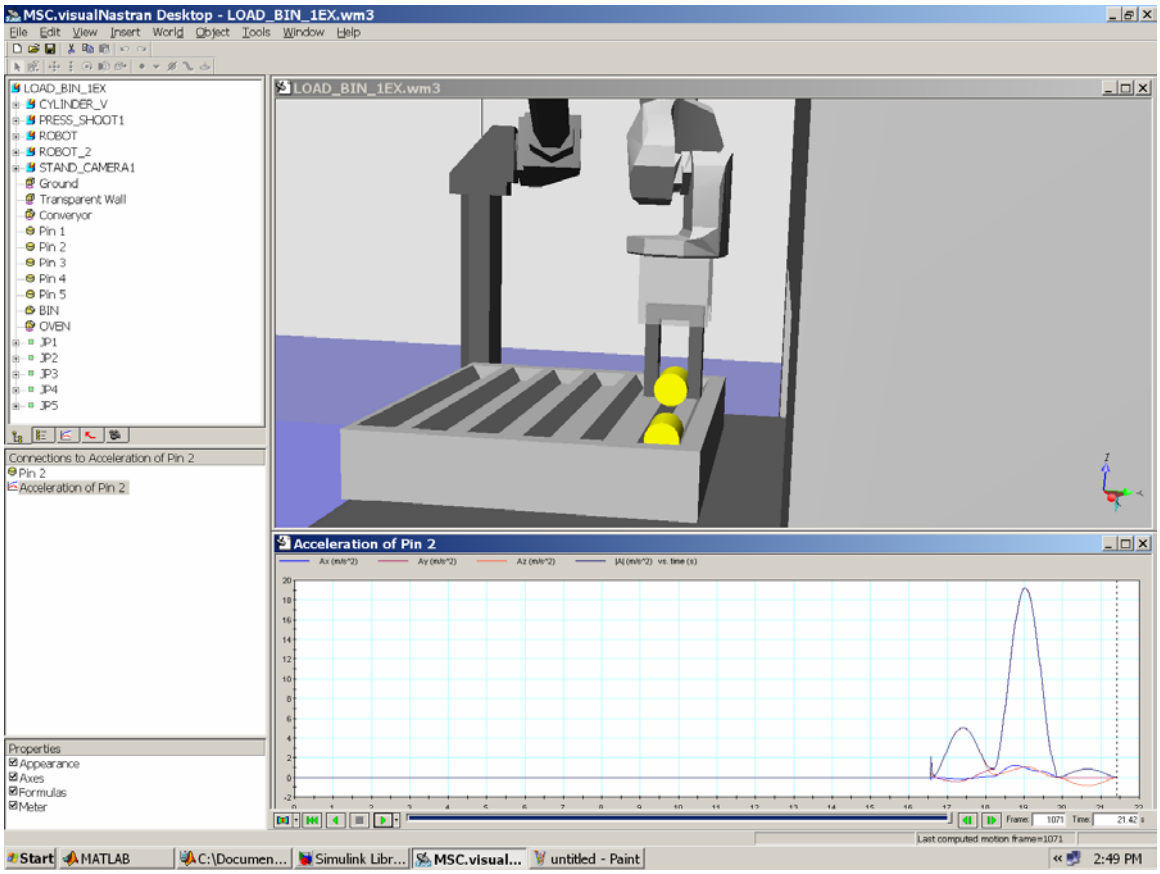


Figure 3.4. A pellet being placed in the boat prior to sintering. The pellet's acceleration did not exceed 20 m/s$^2$ as designed.

Moving one pellet to the grinder takes 6 seconds, as well as 4 seconds to travel back and move another pellet. The overall time for 30 pellets will be 296 seconds. For 5 pellets, the time should be 50 seconds. The simulation time was observed as 50.5 seconds.

After grinding, the pellets are placed in the V-Tray for insertion in the cladding tube. Each pellet has to be inspected individually by a camera before being placed into the V-Tray. The manipulator can move each pellet in 6 seconds, including 2 seconds for the camera inspection. For 30 pellets, the manipulator needs 269 seconds to achieve this task. Again, the highest acceleration attained by any pellet is 20 m/s$^2$.

Depending on the process, sintering can take from 2 to 24 hours to heat-treat 30 pellets. This time element is clearly dominant, and one would assume that several trays would be present in the oven any time. Operational safety would be ensured through spatial separation and possibly additional barriers between boats.

*Conclusion*

A scientific throughput of a hot cell designed and described in past reports was fully analyzed and studied. The cycles were studied theoretically using the manipulator's kinematics. The simulation in MSC.visualNastran© environment shows very close results to those obtained analytically. The next step in our project will be to model the metallic fuel process in the same 3D environment that was used for the powder processing cell.

*Object Recognition*

Further refinements were made to the object recognition tools developed by Dr. J.K. Lee. The focus was on porting the segmentation and adaptive filtering for contour detection in CCD images to Matlab. This work was performed by Ms. Caroline Wiejak of ESIEE, Marne-la-Vallee. Fig. 3.5 shows an example of successful image processing and object identification performed in Matlab.

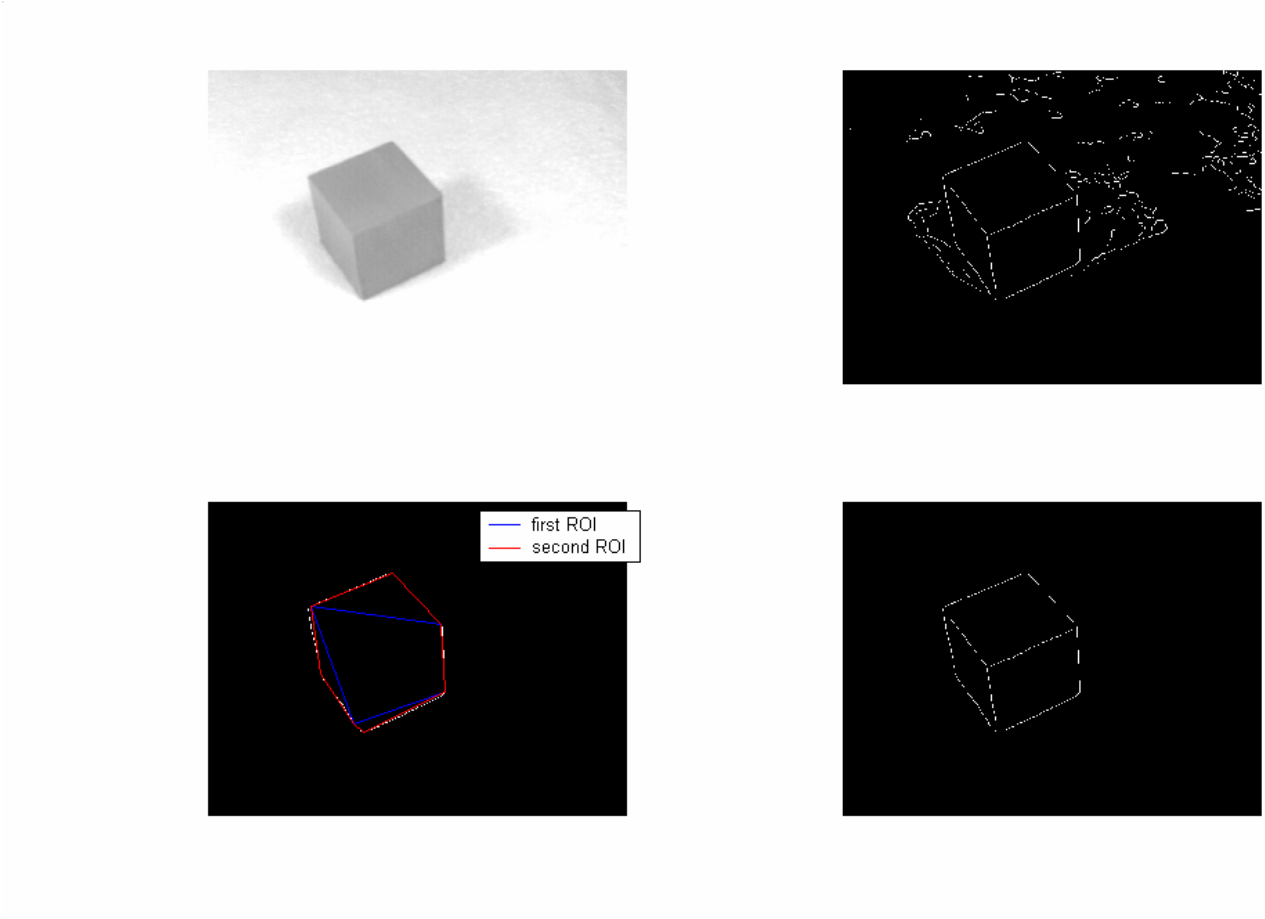


Figure 3.5. Machine Recognition in Matlab. (Top Left: Original Photograph, Top right: Segmented Image containing Noise, Bottom Left: Steps of the Object Identification Process, Bottom Right: Object is correctly identified as a cube.)

## TRANSMUTATION SCIENCES

**LBE Corrosion Modeling (Task 5)**. One of the critical obstacles to the wide use of LBE as a nuclear coolant is corrosion. Unprotected steel undergoes severe attack by liquid lead and lead-bismuth alloy by dissolution of its components in the liquid metal. The present study involves the estimation of corrosion in the liquid metal by imposing an analytically developed concentration expression on the wall surfaces and benchmarking the CFD tool and performing a series of parametric studies on the loop model. The concentration and temperature diffusions due to different flow regimes have been studied. Regions of maximal corrosion and precipitation have been deduced from the simulations and the results have been compared with the analytical models.

*Numerical Simulation Technique*

The STAR-CD computer simulation code was chosen for the purpose of performing the Computational Fluid Dynamics (CFD) calculations for this project. The code is a transient multidimensional simulator for thermal hydraulics and chemical reactions occurring in the fluid

flow itself. STAR-CD is a general-purpose code that solves numerically a set of differential equations that describe the following conservation laws: mass conservation, momentum, energy and chemical species.

*T-joint*

The tee-joint model was constructed using the modeling package SOLIDWORKS. The mesh is made using PRO-AM. The simulated results were obtained for both the laminar and the turbulent flows. A one-inlet, two-outlets model is considered. The first model has inlet at the side and the second model has the inlet in the middle.

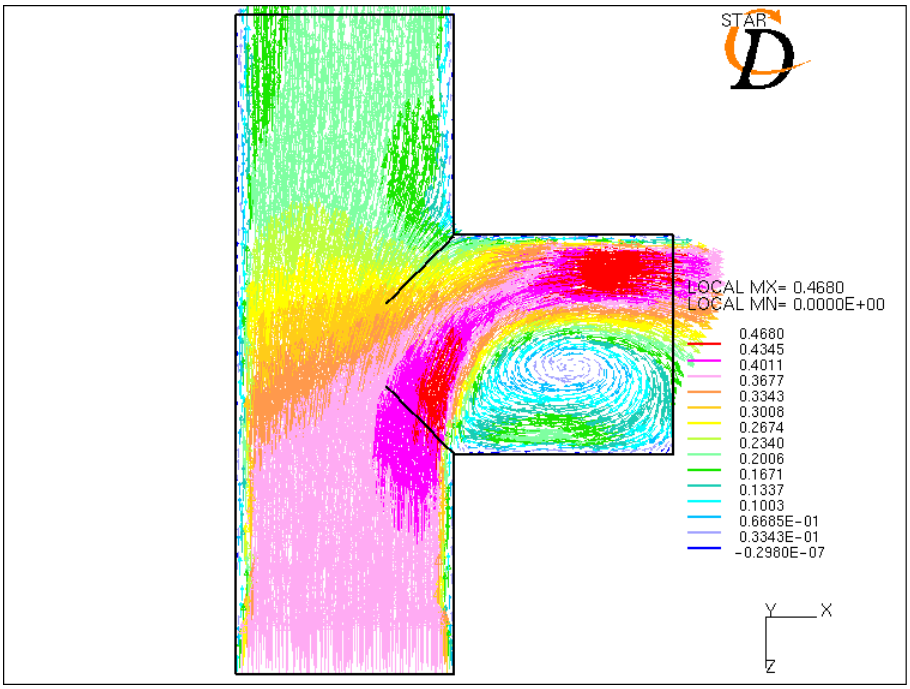


Figure 3.6: Velocity vectors for a side inlet (from bottom inlet) t-joint at Re = 200,000 (turbulent flow)

Figure 3.6 shows the flow patterns at Reynolds number is 200,000. Here a prominent flow reversal of the fluid can be seen in the inner branch of the middle inlet. On the opposing wall of where the eddy current occurs, an area formed where the velocity magnitude increases. This is because of pressure drop.

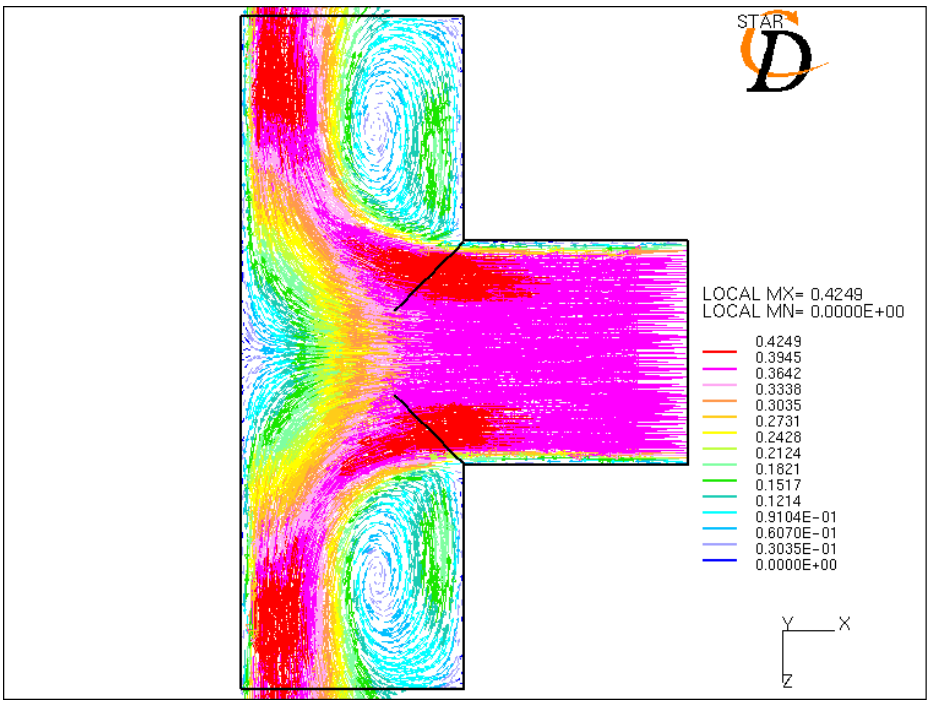


Figure 3.7. Velocity vectors for a middle inlet t-joint at Re = 200,000 (turbulent flow).

Figure 3.7 shows the flow patterns when the inlet is through the middle arm. The velocity vectors are larger in magnitude at the outer wall just after going through the tee intersection on both sides. These bigger velocity vectors then move toward the outlets. The cause of the bigger velocity vectors at these locations seems to be the pressure drop at these locations and there is no back flow or increased pressure areas between these locations and the outlets to slow down the flow. Directly above these areas of bigger velocity magnitude, two areas of smaller velocity magnitude can be seen coinciding with the two areas of lower pressure. Figure 3.7 displays the formation of two eddy currents at these locations where the flow actually forms a circular pattern.

*Study of Surface Chemical Reactions*

The CFD domain, material, fluid zones, boundary conditions, each species' inlet concentration, temperature, etc., have been defined. Specifically, a very simple straight pipe (0.0508 m * 0.25 m) 3-D CFD model has been built to serve as a benchmark case. A fluid zone with a thickness of 2.54 mm is used to monitor the concentration change of Fe. The outer surface of this fluid zone is defined as wall boundary condition. It is defined as adiabatic boundary condition and its material is set to be Fe. The bulk fluid inside the piping is also modeled as a fluid zone (the red area in Figure 3.8). In addition, a layer of baffle cells between the monitoring fluid cell zone and bulk fluid cell zones was created. Both sides of the baffle have been defined as adiabatic boundary conditions at this time. They might be changed to diffusion boundary conditions if fluid condition changes.

One end of piping is defined as an 'inlet' boundary condition while the other end is defined as 'outlet' boundary condition. The velocity of inlet is set to be 0.5 m/s which is close to real conditions. The bulk fluid material (so called background material) is set to be lead bismuth eutectic.

A chemical reaction subroutine dealing with surface chemistry has been developed (see Appendix) and been incorporated into the CFD model. The subroutine includes the specific reactions (in this case, $3Fe + 2O_2 = Fe_3O_4$ and $Fe_3O_4 + 4\ Pb = 3\ Fe + 4PbO$) which occur at LBE surface, chemical reaction rate calculation, the species' molecular weights, the initial species' concentration, temperature, iterations, etc. Arrhenius Equation is used to calculate the reactant reaction rate. But some coefficients need to be validated by experimental result if they are available for our specific reactions.

Several run with and without subroutine connected have been made. Figure 3.8 shows velocity profile inside the piping without subroutine connected. It is obvious that this is a laminar flow. The fluid condition inside the pipe will significantly affect the species' diffusion, hence the corrosion process of the piping wall.

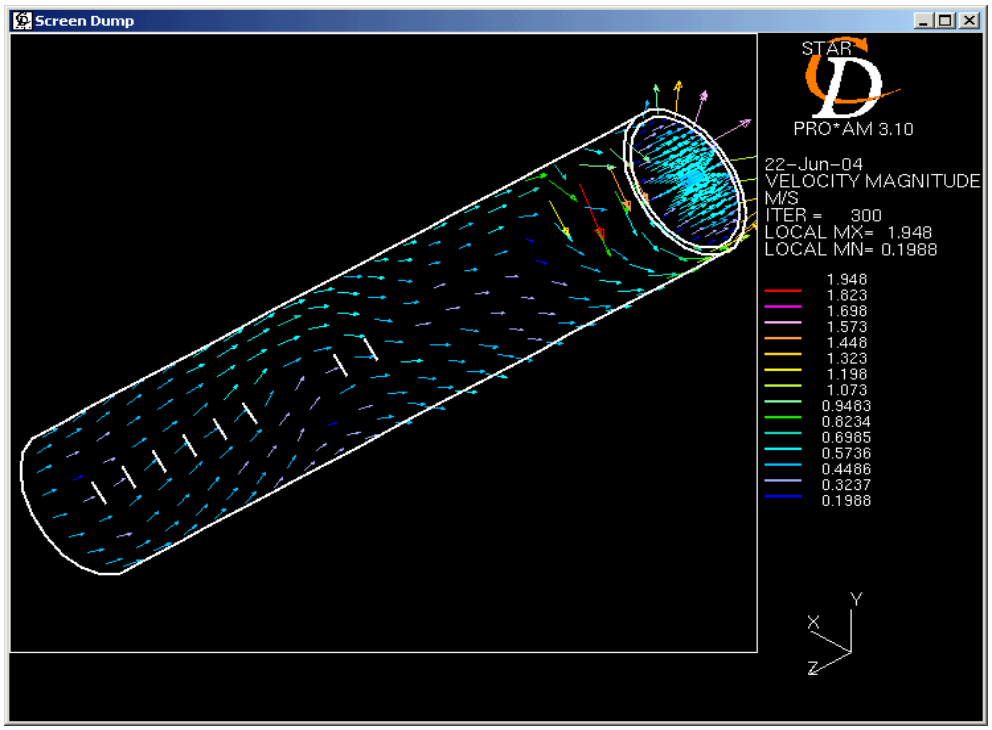


Figure 3.8. Velocity vectors inside the pipe.